GEOPHYSICS, VOL. 71, NO. 2 (MARCH-APRIL 2006); P. G53–G62, 7 FIGS., 1 TABLE.
10.1190/1.2187752

Robust 1D inversion and analysis of helicopter electromagnetic (HEM) data

Rasmus Juhl Tølbøll[1] and Niels Bøie Christensen[1]

ABSTRACT

Ground-based electrical and electromagnetic methods are used systematically for quantitative hydrogeologic investigations in Denmark. In recent years, a desire for faster and more cost-efficient methods has led to growing interest in the possibility of using airborne systems, and in 2001 a number of test flights were performed using a frequency-domain, helicopter-borne electromagnetic (HEM) system.

We perform a theoretical examination of the resolution capabilities of the applied system. Quantitative model parameter analyses show that the system only weakly resolves conductive, near-surface layers but can resolve layer boundary to a depth of more than 100 m. Modeling experiments also show that the effect of altimeter errors on the inversion results is serious.

We suggest a new interpretation scheme for HEM data founded solely on full nonlinear 1D inversion and providing layered-earth models supported by data misfit parameters and a quantitative model-parameter analysis. The backbone of the scheme is the removal of cultural coupling effects followed by a multilayer inversion that in turn provides reliable starting models for a subsequent few-layer inversion. A new procedure for correlation in the model space ensures model sections with slow lateral variations in resistivity, normally assumed in sedimentary environments.

A field example from a Danish survey demonstrates that the interpretation scheme can produce satisfactory results within the limitations of the system.

INTRODUCTION

Groundwater provides an essential resource for agriculture and industry in Denmark, and it is also the principal source of drinking water (Christiansen and Sørensen, 1998.) However, its quality is seriously threatened by intensive farming and increased pumping rates, especially in urbanized areas. High-quality groundwater resources have therefore steadily depleted, and frequent contamination has caused numerous waterworks to shut down.

A large-scale hydrogeologic project has been conducted to map available aquifers and their vulnerability in order to provide a detailed, informed basis for future water policy decisions. Ground-based electric and EM methods are successfully applied for this mapping campaign. Typically, the transient electromagnetic (TEM) method is used to delineate the lower, impermeable aquifer boundaries (Poulsen and Christensen, 1999; Danielsen et al., 2003), whereas continuous electrical methods [continuous vertical electrical sounding (CVES) and pulled-array continuous electrical sounding (PACS)] are utilized for mapping near-surface clay characterizing aquifer vulnerability (Sørensen, 1996). However, the move toward faster and more cost-efficient methods for hydrogeologic investigations has led to growing interest in the possibility of using airborne electromagnetic (AEM) methods, and different systems have been tested (Christiansen and Christensen, 2003; Sørensen and Auken, 2003). Recently, attention has been paid to the frequency-domain helicopter-borne electromagnetic (HEM) methods, and in 2001 a series of trials were conducted in Denmark.

Traditionally, HEM data are interpreted by the pseudolayer half-space model algorithm developed by Fraser (1978). This algorithm is based on computed lookup tables and provides two interpretation parameters—apparent resistivity and apparent depth—from the EM response of a single frequency. The newer centroid depth concept (Sengpiel, 1988) takes multifrequency data sets as input. Assigning specific depths to the apparent resistivities, it transforms the data set into a sounding curve, thus yielding a smooth image of the vertical earth resistivity structures. Similar methods with different sensitivity to vertical resistivity contrasts have been developed and used on a regular basis, e.g., the differential parameter method (Huang and Fraser, 1996) and enhanced sounding curves (Siemon, 2001).

Recent literature focuses on full, nonlinear, iterative 1D inversion of AEM frequency-domain data. Beard (2000)

Manuscript received by the Editor June 24, 2004; revised manuscript received May 8, 2005; published online March 9, 2006.
[1]University of Aarhus, Department of Earth Sciences, Finlandsgade 6-8, DK-8200 Aarhus N, Denmark. E-mail: tolboll@geo.au.dk; nbc@geo.au.dk.

calculates a half-space resistivity from a single data frequency using a damped least-squares formalism and concludes that the method is often preferable to the Fraser half-space method. Likewise, Beamish (2002a) performs 1D inversion of both theoretical and survey data from the dual-frequency fixed-wing system from the Geologic Survey of Finland (GTK). Half-space resistivities are deduced from the frequency data, and two-layer inversion is performed successfully on the basis of the combined data set. A procedure for full, nonlinear 1D inversion of multifrequency data, but with starting models derived from the results of approximate transforms, is presented by Sengpiel and Siemon (1998). They test this inversion procedure (2000) on synthetic and survey data and optimize it with respect to starting-model selection. These experiments indicate that inversion of data from sedimentary environments can be performed successfully using an inversion procedure, whereas data from complex resistivity structures are better represented applying approximate transforms.

In this paper, we present a theoretical study of the resolution capabilities of a multifrequency HEM system. Our main objective is to examine whether it is applicable for mapping near-surface capping clay (estimation of aquifer vulnerability) and delineating of the lower impermeable boundaries of potential aquifers. These are two main areas of interest in hydrogeologic investigations in a layered sedimentary environment such as Denmark. The examination of the resolution capabilities is based on quantitative parameter analyses of 1D earth models. Special attention is given to the altitude parameter and the formulation of a noise model describing the uncertainty of the individual data points. The latter is a requisite for reliable quantitative analysis and inversion.

We also present a new, robust inversion scheme for multifrequency HEM data based on full, nonlinear 1D inversion. This scheme provides reliable earth models with supporting data-misfit parameters and quantitative model parameter analysis of resolution. A lateral correlation in the model space is performed to ensure model sections with the slow lateral variations in geology normally associated with sedimentary environments. Finally, we discuss the effect of EM coupling to man-made conductors (cultural coupling) and demonstrate the applicability of the inversion scheme by inverting a data set from a Danish survey.

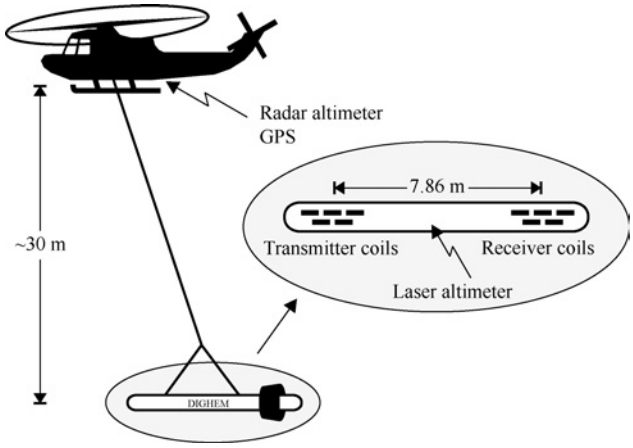

Figure 1. Schematic of the HEM system.

Table 1. The absolute noise (in ppm) on the five frequencies of the HEM system. The total absolute noise, $noise_{abs}^{total}$, is the sum of stochastic noise, $noise_{abs}^{stoc}$, and a noise contribution accounting for the nonlinear drift, $noise_{abs}^{drift}$.

Frequency [Hz]	$Noise_{abs}^{stoc}$	$Noise_{abs}^{drift}$	$Noise_{abs}^{total}$
380	5	3	8
1500	5	3.75	8.75
6200	10	6	16
25 700	20	9	29
102 000	25	13.5	38.5

SYSTEM SPECIFICATIONS

All analyses in this paper are based on the DIGHEM^{VRES} system, a frequency-domain HEM system using five horizontal coplanar magnetic dipole-dipole configurations (see Figure 1). It operates at frequencies of 0.38, 1.5, 6.2, 25.7, and 102 kHz; the coil separation is 7.86 m for all five coil pairs. Both the transmitter and the receiver coils are mounted in a cylindrical kevlar bird suspended approximately 30 m below the helicopter. The bird's altitude is measured directly by a laser altimeter inside the bird. It is also obtained independently by subtracting the presumed vertical distance between the helicopter and the bird from the helicopter's altitude, as determined by a radar altimeter. The nominal bird height above ground is 30 m.

During the flight the secondary magnetic field for each frequency is measured by the receiver coils, with five bucking coils compensating the primary fields. The coupling ratio, defined as the secondary to the primary field, is split into its real (in-phase) and imaginary (quadrature) parts and is registered in parts per million (ppm). The data-acquisition rate is 10 Hz, equivalent to an approximately 3-m, along-line sampling distance at a typical survey speed of 110 km/hour. During flight, at approximately 20-minute intervals, the zero level is found through high-altitude measurements, and the measured data residual is established as the system zero level.

Noise model

A quantitative estimate of the individual data uncertainty, known as a noise model, is needed to accomplish meaningful inversions and model-parameter analyses. We have formulated a standard noise model for the DIGHEM^{VRES} system based on accessible system specifications. All inversions and analyses presented in our paper refer to this model.

The standard noise model assumes that the absolute noise level of the individual measurements is the sum of a stochastic noise contribution and a contribution accounting for an inadequate drift correction. The stochastic noise results from ambient noise, inherent instrumental noise, and mechanical vibrations causing stochastic noise, both directly by affecting the rigid coil geometry and indirectly by jarring the metallic bird parts. The estimated stochastic noise, $noise_{abs}^{stoc}$, at each of the five frequencies is estimated as half of the typical peak-to-peak noise (see Table 1).

In the data-processing stage, the system drift is assumed to be linear between the high-altitude checks. However, this

is not necessarily the case. Because of altitude changes, it is likely for the major part of the drift to take place during the calibration checks. In the standard noise model the nonlinear drift component is estimated to be 15% of the typical drift. The estimated noise contributions, $\text{noise}_{\text{abs}}^{\text{drift}}$, accounting for nonlinear drift are listed in Table 1. The total absolute noise, $\text{noise}_{\text{abs}}^{\text{total}}$, at the five frequencies is seen also in the table.

In addition to absolute noise, the data are assigned another 5% relative noise to account for errors introduced in the model when assuming one dimensionality and to allow for deviations from the nominal system configuration. The relative noise contribution, $\text{noise}_{\text{rel}}$, is calculated as

$$\text{noise}_{\text{rel}} = 0.05\,(R^2 + I^2)^{1/2}, \tag{1}$$

where R is the real part and I is the imaginary part of the registered coupling ratios.

MODELING, INVERSION, AND ANALYSIS

All computations are performed using the SELMA program (Christensen and Auken, 1992), and associated utilities SELMA is a tool for model-response calculations, analysis, and inversion of the most common ground-based and AEM data types. The basic model is a 1D layered half-space consisting of horizontal, homogeneous, and isotropic layers.

The inversion problem is solved using the well-established iterative damped approach (Menke, 1989). Formally, the model update at the nth iteration is given by

$$\begin{aligned}\mathbf{m}_{n+1} = \mathbf{m}_n + &\left[\mathbf{G}_n^T\mathbf{C}_{\text{obs}}^{-1}\mathbf{G}_n + \mathbf{C}_{\text{prior}}^{-1} + \mathbf{R}^T\mathbf{C}_R^{-1}\mathbf{R} + \lambda\mathbf{I}\right]^{-1} \\ &\times \left[\mathbf{G}_n^T\mathbf{C}_{\text{obs}}^{-1}(\mathbf{d}_{\text{obs}} - \mathbf{g}(m_n)) \right. \\ &\left. + \mathbf{C}_{\text{prior}}^{-1}(\mathbf{m}_{\text{prior}} - \mathbf{m}_n) + \mathbf{R}^T\mathbf{C}_R^{-1}(-\mathbf{R}\mathbf{m}_n)\right], \end{aligned} \tag{2}$$

where $\mathbf{m}$ is the model vector containing the logarithm of the model parameters, $\mathbf{G}$ is the Jacobian matrix containing the derivatives of the data with respect to the model parameters, T is the vector transpose, $\mathbf{C}_{\text{obs}}$ is the data error covariance matrix, $\mathbf{C}_{\text{prior}}$ is the covariance matrix on the prior model, $\mathbf{R}$ is the roughening matrix containing 1 and -1 for the constrained parameters and 0 in all other places, $\mathbf{C}_R$ is a covariance matrix describing the constraint strength, λ is the Marquard damping factor, $\mathbf{I}$ is the identity matrix, $\mathbf{d}_{\text{obs}}$ is the field-data vector, $\mathbf{g}(m_n)$ is the nonlinear forward-response vector of the nth model, and $\mathbf{m}_{\text{prior}}$ is the prior-model vector. The data noise (described by the noise model) is assumed to be uncorrelated, implying that $\mathbf{C}_{\text{obs}}$ is a diagonal matrix.

Our interpretation strategy for HEM data uses both few-layer and multilayer inversions. In few-layer inversion, layer resistivities and thicknesses are free to vary and no model parameter constraints are applied, corresponding to an exclusion of the $\mathbf{R}$-term in equation 2. Generally, the few-layer inversion minimizes the data misfit using a specific, small number of layers. In the multilayer inversion, the layer boundaries are totally fixed, and only the layer resistivities are free parameters. The inversion is regularized through vertical constraints (the $\mathbf{R}$-term in equation 2), ensuring identity between neighboring layer resistivities within a given relative uncertainty. To obtain more blocky models, the optimization problem is solved with an L_1-norm (Farquharson and Oldenburg, 1998), whereas a traditional L_2-norm is used in the few-layer case.

The model-parameter analysis relies on a linear approximation to the posterior covariance matrix $\mathbf{C}_{\text{est}}$, given by

$$\mathbf{C}_{\text{est}} = \left[\mathbf{G}^T\mathbf{C}_{\text{obs}}^{-1}\mathbf{G} + \mathbf{C}_{\text{prior}}^{-1} + \mathbf{R}^T\mathbf{C}_R^{-1}\mathbf{R}\right]^{-1}, \tag{3}$$

where $\mathbf{G}$ is based on the final model. The analysis is given by the standard deviations of the model parameters, obtained as the square root of the diagonal elements of $\mathbf{C}_{\text{est}}$ (Inman, 1975). The linear model parameter analysis will be demonstrated on both synthetic and field data.

RESOLUTION CAPABILITIES

The use of the HEM method for quantitative, hydrogeologic investigations raises questions about its resolution capabilities. Here, we examine the vertical-resolution capabilities on the basis of quantitative model-parameter analysis of 1D earth models. However, we first consider bird altitude. This is an important parameter in the resolution capability analysis because EM responses are strongly correlated to the elevation of the transmitter and receiver coils above ground (Beamish, 2002b).

Altitude parameter

The HEM surveys performed in Denmark are marked by problems in bird-altitude determination. This is mainly because of the canopy effect, i.e., the laser and the radar altimeter being reflected from elevated ground features such as dense tree cover and buildings, resulting in incorrectly low altimeter readings. Altitude measurements are also uncertain because of random fluctuations. Thus, laser-height accuracy is affected by bird movements during the flight, resulting in changes of the laser angle to the ground. Radar height accuracy is reduced mainly by an uncertain estimate of the vertical distance between the helicopter and the bird.

To examine the significance of altitude errors on the inverted models, we compute the model response for a 50-ohm-m half-space at a 30-m bird height and subsequently invert the synthetic data using 21 different altitudes ranging from 25–35 m in 0.5-m steps. The inversions use a multilayer model with bird altitude implemented as a configuration parameter and noise ascribed in accordance with the standard noise model. The applied altitudes and the inversion results are shown in Figure 2. As expected, underestimated altitudes result in overestimated resistivities in the uppermost part of the models and vice versa. Even with a bird altitude just 1 m in error, the output model is disturbed and a clearly wrong interpretation is obtained.

To avoid the disturbing effect of altimeter errors in the inversion, we adopt a method proposed by Beamish (2002b), with the bird altitude entering the inversion scheme as a variable model parameter instead of as a configuration parameter. The method introduces an extra high-resistivity top layer with a thickness representing bird altitude. The layer thickness is free to vary, and the resistivity is tightly constrained with a relative uncertainty of 0.001 to a prior value of 100 000 ohm-m. This method is referred to as the air-layer technique.

In the following, we examine how the air-layer technique affects the determination of model parameters. The examination is based on 21 different three-layer models portrayed in Figure 3a. The layer resistivities are 30, 70, and 5 ohm-m from

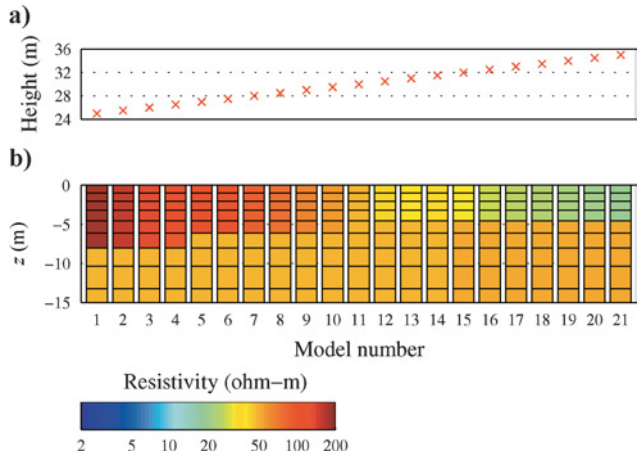

Figure 2. The significance of erroneous height information on the inverted models for a 50 ohm-m half-space. (a) Assumed bird heights used for the inversions. (b) Multilayer inversion results using bird height as a configuration parameter. The fixed-layer boundaries used in the inversion are indicated by the horizontal lines.

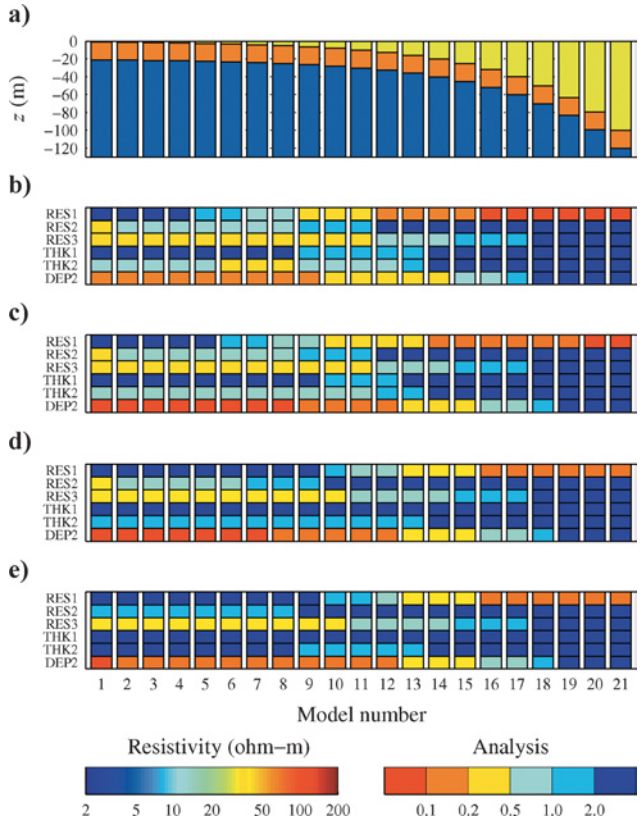

Figure 3. Model parameter analysis of a three-layer model suite. (a) True models; resistivities are indicated by the left color bar at the bottom. (b)–(e) Analysis sections; relative parameter uncertainties are indicated by the right color bar at the bottom. (b) The bird altitude as a configuration, parameter; (c) the air-layer technique, with the bird altitude constrained with an absolute uncertainty of 1 m to the true bird altitude; (d) the air-layer technique, with the bird altitude constrained with an absolute uncertainty of 10 m to the true bird altitude; and (e) the air-layer technique, with no prior information.

top to bottom, and the thickness of the first layer is changed exponentially from 1–100 m with 10 samples per decade, gradually displacing the 30-m-thick second layer to a greater depth. The model suite is intended to represent a clay-rich till overlying limestone with saline groundwater at the bottom, resembling the geologic setting in the survey area addressed below in this paper. Figure 3b shows the model-parameter analysis, with bird altitude entered as a configuration parameter. In addition to the primary model parameters (the resistivities of the first, second, and third layers and the thicknesses of the first and the second layers), the analysis includes the depth to the third layer. The analysis is presented using a discrete color scale, with reds representing well-determined parameters (low standard deviations) and blues representing poorly determined parameters (high standard deviations). Figures 3c–3e present the model-parameter analysis using the air-layer technique. In Figures 3c and 3d the true bird height (35 m) enters as a prior value with absolute uncertainties of 1 and 10 m, respectively, whereas in Figure 3e the bird altitude is unconstrained. As expected, the model parameter determination is degraded when bird altitude is included as a model parameter instead of as a configuration parameter. However, the deteriorations are quite moderate. Prior information on bird altitude with an uncertainty of 1 m (Figure 3c) leads to a generally unchanged analysis, and only a limited reduction occurs with a 10-m uncertainty (Figure 3d) or a bird altitude totally free to vary (Figure 3e).

The analysis demonstrates that very little information is lost when the air-layer technique is implemented. This is because the resistivity of the extra air layer is completely fixed, while the adjustable thickness parameter is very stable to resolve. The analysis also shows that including prior information on the air-layer thickness has only a minor positive effect on model-parameter resolution.

Another approach to overcome the problem of incorrect bird altitude is presented by Hodges (2003). This technique includes bird altitude as an independent parameter that can be adjusted during inversion without introducing an extra air layer. For practical purposes there is no substantial difference between this technique and the air-layer technique, because in the latter the resistivity of the extra air layer is completely fixed, leaving only bird altitude as a real variable.

Model-parameter analysis

Figure 4 shows the model-parameter analysis of a two-layer model suite using the air-layer technique. Generally, more than two layers are required for modeling the actual geologic settings, but this simple model is useful when appraising some fundamental system characteristics, e.g., the depth to which earth structures can be resolved (penetration depth) and the capabilities of resolving near-surface clay layers (estimation of aquifer vulnerability). Moreover, it presents an exhaustive parameter analysis concisely.

The analysis in Figure 4 is shown as contours or templates (Christensen and Sørensen, 2001) of the standard deviations of the primary model parameters using the same discrete color scale as in Figure 3. In each template the resistivity of the first earth layer (RES1) varies from 1–100 ohm-m and the thickness of the first layer (THK1) varies from 1–100 m. Both parameters are changed exponentially in 21 steps with

10 samples per decade, giving rise to 441 models in each template. The resistivity of the second layer (RES2) also changes exponentially from 1–100 ohm-m but with only two samples per decade, and for each parameter value a distinct template is produced.

The analysis of RES1 is shown in Figure 4a. The RES1 determination is strongly dependent on THK1, as the parameter is totally undetermined for small THK1 values but well determined for high values. The determination of RES1 is also affected, but to a much lesser extent, by the specific value of the parameter itself. Even under optimal conditions, a THK1 value of more than 3 m is required to achieve a relative uncertainty of RES1 less than 0.5. Figure 4b demonstrates that RES2 is relatively well determined only for the combination of small THK1 and high RES1 values. The RES2 determination improves overall with decreasing values of the parameter itself, but the standard deviation of RES2 is nowhere below 0.1. The analysis of the last primary model parameter, THK1, is presented in Figure 4c. The best THK1 determination appears to be obtained only in a limited interval of THK1 values. The interval extent is strongly dependent on the RES2 value, with low RES2 values resulting in the best determination. Note that the determination of THK1 is only weakly dependent on RES1, apart from the parameter being totally undetermined when the contrast between RES1 and RES2 is low.

In general terms, the near-surface protective layers in Denmark consist of Quaternary clay with resistivities of 30–60 ohm-m, whereas the underlying aquifers are characterized by higher resistivities of typically 50–100 ohm-m, depending on the resistivity of the pore water and the water-bearing material. To be useful for estimation of aquifer vulnerability, the HEM system must be able to resolve both the resistivity and the thickness of the conductive clay layer within the uppermost 50 m of the earth. The model-parameter analysis clearly demonstrates that this is impossible. For thin clay layers, both the thickness and the resistivity parameters are undetermined, and with increasing layer thickness the thickness remains undetermined.

The lower hydrologic boundary of the aquifers generally consists of very low-resistivity Tertiary clay or saltwater. The model-parameter analysis shows that the HEM system in the best case can resolve such layers to more than 100 m depth.

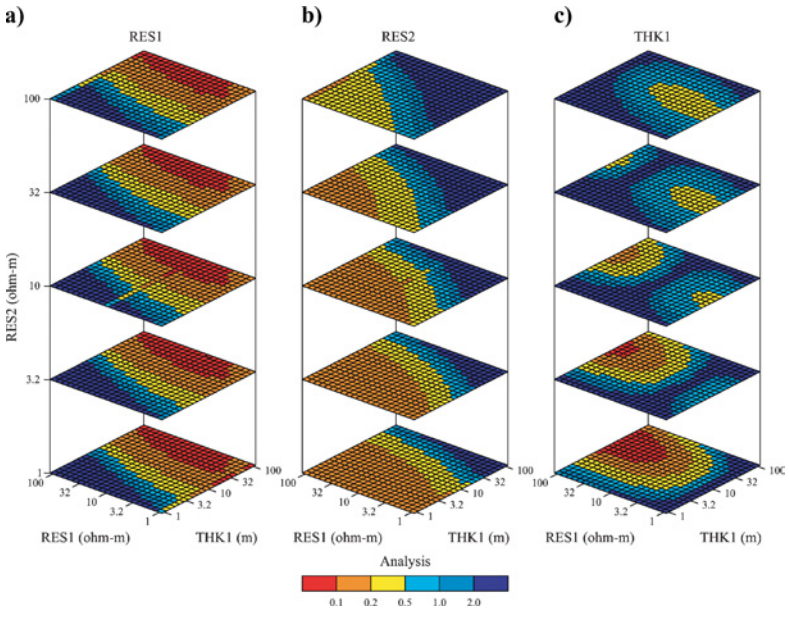

Figure 4. Theoretical model-parameter analysis of a general two-layer model. Analysis for (a) the resistivity of the first layer (RES1), (b) the resistivity of the second layer (RES2), and (c) the thickness of the first layer (THK1).

INVERSION OF HEM DATA

In summer 2001, several HEM surveys were conducted in Denmark. Based on the acquired survey data, we developed a new inversion scheme founded on full nonlinear 1D inversion, presented here with a field example from one of the survey areas. Before presenting the results, we briefly describe the survey area and data and discuss the problem with cultural coupling.

Survey area and data

The survey area covers most of Stevns a peninsula located in the eastern part of Zealand, south of Copenhagen. Geologically, the area is characterized by Quaternary deposits overlying a thick Tertiary and Cretaceous limestone package. The Quaternary overburden is till, mainly clay, from less than 5-m and up to 30-m thick. Salt groundwater in the deeper limestone is reported in boreholes (Jakobsen et al., 1997).

The survey data were collected along 48 lines flown from southwest to northeast with a 200-m nominal line spacing, totaling an approximately 187-km^2 area. Control lines were flown perpendicular to the primary lines, with 2-km spacing.

The data set includes both raw and processed EM data. In the data-processing stage, the drift was removed from all data channels and the data were shifted manually on the basis of the control lines (leveling). Finally, filtering was performed, applying a median filter followed by a Hanning filter. The filter operator length for both filters was 51 readings, corresponding to a lateral scale length of approximately 150 m.

In this paper we concentrate on line 10 010 from the northwestern part of the survey area. Relevant data from this 7.5-km-long line are presented in Figure 5. The bird-altitude measurements (Figure 5a) indicate altitudes between 25 and 50 m. Two features are especially notable: (1) an approximately 5-m offset between the registered laser and radar heights along the major part of the profile, possibly from poor estimates of the helicopter-bird separation, and (2) a number of rapid fluctuations in the laser measurements, most prominent at coordinates from 3000–3200 m and at the very beginning of the profile (0–200 m). Both features illustrate the problem with the bird-altitude measurement and accentuate the need for special focus on this parameter. The processed real and imaginary parts of the EM responses along the profile are shown in

Figures 5b and 5c. For all data channels, the variations along the profile are of relatively long wavelength because of the filtering, and they appear to be caused mainly by changes in bird altitude. Finally, Figure 5d presents an approximate image of the subsurface resistivity distribution using the differential-parameter method developed by Huang and Fraser (1996). The differential-resistivity section, based on differential resistivities and differential depths, reveals a highly resistive homogeneous layer underlain by a more conductive bottom layer. The boundary between the two layers is a smooth transition, and no precise, well-defined depth to the bottom layer is seen. However, there is no doubt that the thickness of the first layer varies considerably along the profile. Geologically, the differential resistivity section is interpreted as limestone, with the low resistivity in the lower parts caused by saltwater intrusions. There are no indications of the conductive Quaternary overburden.

Cultural coupling

During HEM measurements, currents are induced not only in the earth but also in any conducting man-made structures in the vicinity of the measuring system, e.g., power lines, buried cables, and railway tracks. This coupling to man-made conductors is a serious source of data error, as the magnetic fields induced by the currents lead to significant distortions of the registered responses. Thus, it can be detrimental to the interpretation of HEM data, especially in densely populated areas intersected by disturbing structures.

In a layered sedimentary environment with only moderate lateral geologic variations, the EM responses along a survey line are long waved. In contrast, man-made disturbances are typically seen as narrow, rapid oscillations that are not produced by geologic sources. Theoretically, the cultural coupling manifests itself as a clear, symmetrical M-shape whenever an elongated wire is crossed (Fraser, 1987; Siemon et al., 2002). The situation is blurred more for field data, but the cultural coupling nevertheless is recognized often and easily in the data profile. This is illustrated in Figures 6a and 6c, showing the real and imaginary parts of the raw data for the three-lowest frequencies along a small section of line 10 010. A double-peaked anomaly exists in both the real and imaginary parts, indicating a cultural coupling centered at coordinate 3780 m. The shapes of the affected data responses do not reveal the origin of the disturbance, but comparison with infrastructure maps shows that this particular cultural coupling is caused by a buried cable.

The main purpose of the filtering performed in the data-processing stage is to remove nongeologic noise from the raw data. The filtering is indeed effecitve for stochastic noise; unfortunately, it cannot remove the deterministic source responses of cultural couplings. This is indicated in Figures 6b and 6d, showing the real and imaginary parts of the processed data along the same line as before. The cultural coupling appears to be somewhat subdued, but it is still recognizable as a small upward bulge in the data. Moreover, the filtering has the undesirable effect of extending the cultural coupling laterally, distorting a larger part of the data set. Consequently, data affected by cultural coupling need to be culled from the data before the inversion — preferably in the data-processing stage before filtering.

In this study, the identification and registration of cultural couplings is based on manual inspection of the raw data and associated noise tracks, which are computed by band-pass filtering of the real parts at each frequency. In total, the data set reveals almost 700 cultural couplings; most can be associated with known cultural infrastructures in the survey area. The effect of the cultural coupling extends to all frequencies, but generally it is most pronounced in low-frequency data where the coupling to powerlines mainly occurs. However, a wide variety of coupling responses occurs, and in some cases the coupling effect is seen predominantly in the high-frequency data. In Figure 5c the locations of the manually identified cultural couplings along line 10 010 are marked by vertical arrows below the data. The differential-resistivity section in Figure 5d is clearly influenced by the cultural couplings. Thus, the calculated differential depths are generally reduced close to the cultural couplings, and in some cases the resistivities fluctuate remarkably. The example clearly underlines the necessity of removing coupling-affected data to achieve reliable inversion results.

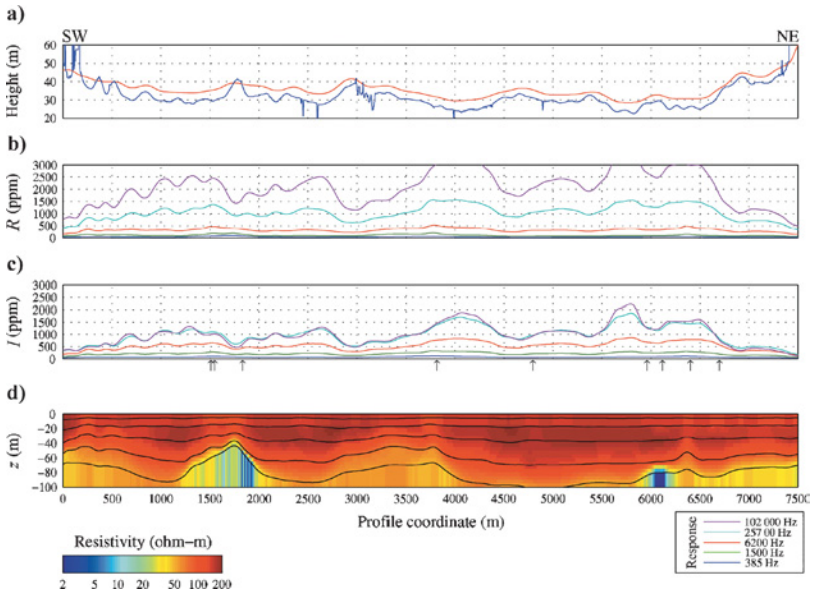

Figure 5. Data and differential section along line 10 010. (a) Measured radar (red) and laser (blue) bird altitude. (b) Processed real and (c) imaginary parts for the five frequencies. (d) Differential section plotted to a depth of 100 m, with differential depths marked by black lines. The arrows below (c) indicate the location of the identified cultural couplings.

New inversion scheme

With modern computers, full nonlinear 1D inversion of multifrequency HEM data can be performed within an acceptable time span. However, the formulation of an automatic inversion procedure for large-volume data sets is not straightforward. First, the restricted resolution capabilities of the HEM system and problems with nonunique solutions imply that a reasonable choice of starting models is necessary for the inversion to succeed. Second, it follows from the 1D assumption that the individual data set is inverted, irrespective of its neighboring data sets. Thus, neighboring models may differ considerably because of the random noise on data; a lateral correlation is therefore required to achieve model sections representing the slow lateral-resistivity variations associated with layered sedimentary environments. Finally, it is difficult to produce a robust routine that runs without breakdowns. This is important because the huge data sets associated with HEM surveys do not allow for personal attention to the individual inversions.

Our inversion scheme is founded solely on full nonlinear 1D inversion. It provides reliable output models, and model reliability is assessed by misfit parameters and model-parameter analyses. The bird-altitude registrations are completely ignored as a result of their unreliability; instead, the air-layer technique is applied. Finally, data affected by cultural coupling are removed from the data set before the inversion. Data from an interval of ±50 measuring points (approximately ±150 m) centered at the midpoint of the identified cultural coupling are removed. The inversion scheme itself is a stepwise procedure, described and illustrated by the results from line 10 010.

Step 1: Multilayer inversion

The first step in the inversion strategy is a multilayer inversion. The purpose is to obtain a first, quantitative image of the earth resistivity distribution from which reasonable starting models for a subsequent few-layer inversion can be extracted.

Because of restrictions in the SELMA program, the bird-altitude parameter must be included in the multilayer inversion as a configuration parameter. This implies that the air-layer technique cannot be implemented. Since we do not want to use bird-altitude measurements in the inversion, an estimate must be provided beforehand. This is obtained through a homogeneous half-space inversion. Only data from the highest frequency are used, and with the air-layer technique implemented, bird altitude is estimated as the thickness of the uppermost air layer in the output model. Utilizing this inverted bird altitude, the multilayer inversion initiates with constant layer resistivities equivalent to the half-space resistivity obtained by the half-space inversion.

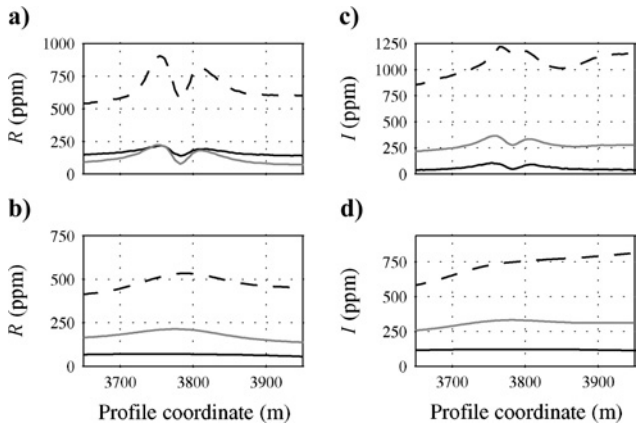

Figure 6. A small section of line 10 010 showing the 380-Hz (black line), 1500-Hz (gray line), and 6200-Hz (dashed line) data. (a) Raw and (b) processed real part. (c) Raw and (d) processed imaginary part.

The multilayer inversion of the field data from line 10 010 uses a 20-layer model with constant smoothness constraints of 0.55 and layer thicknesses increasing with depth as a hyperbolic sine function. The size of the smoothness constraints, which describes the degree of vertical smoothing of the layer resistivities (see equation 2), and the layer thicknesses are pragmatically chosen on the basis of modeling experiments. The result of the inversion is presented in Figure 7a. It reveals a clear, three-layer structure with a thin top layer, a relatively resistive second layer, and a conductive third layer. The layer boundaries are well defined overall; but at the beginning (500–700 m) and in the middle (3 300–3 500 m) of the profile, it is difficult to differentiate between the upper-two layers, indicating that the capping clay may be absent. The low-resistivity bottom layer is relatively inhomogeneous, with resistivities varying considerably along the profile; at coordinates 5000 and 5600, the layer seems to be missing. Finally, the bird altitude used for the inversion provides a reasonable estimate of the actual bird altitude. The calculated height is generally identical to the measured laser height, but the fluctuations are removed.

As stated by other authors (e.g., Fitterman, 1998), the highest-frequency data are generally the most likely to be affected by calibration errors. Therefore, it might be better to use the second-highest frequency data for bird-altitude estimations in routine inversion. However, for the Stevns survey the best results are obtained using the highest-frequency data, as these are not markedly disturbed by calibration errors.

Step 2: Few-layer inversion with extracted starting models

The second step of the inversion strategy transforms the multilayer models from step one into few-layer models. In this process, the number of layers in the resulting few-layer models is first decided; the best few-layer models are then extracted based on a least-squares criterion (see Appendix A). The extracted models are used as starting models for a few-layer inversion with the air-layer technique and the bird height estimate from step 1.

The result of the three-layer inversion with extracted starting models is presented in Figure 7b. The model section is quite similar to the multilayer section (Figure 7b), but it shows a more homogeneous bottom layer and the thicknesses of the two-top layers is overall increased. As expected from the theoretical resolution capability examination, the quantitative analyses of the inverted model sections indicate the model parameters are generally undetermined. Only the depth to the conductive third layer is relatively well determined, with a relative uncertainty below 0.5 in most cases. This relatively poor model-parameter analysis favors a two-layer model, but the

use of a three-layer model for the inversion is justified by the geologic knowledge of the survey area.

Step 3: Few-layer inversion with correlated starting models

Based on the few-layer inversion results from step 2, a correlation in the model space is performed. The purpose is to ensure a model section with the slow lateral-resistivity variations normally found in a layered, sedimentary environment. The correlation is done by predicting new model-parameter values from the set of inverted models using an inversion approach. The new, correlated values are used as prior information in a subsequent few-layer inversion with an uncertainty likewise predicted from the set of inverted models (see Appendix B). Again the air-layer technique is applied.

In the field example, a weight factor of 0.5 for all relevant model parameters and a 5000-m correlation length are used for the correlation. The result of the subsequent inversion with the correlated starting models is presented in Figure 7c. The model section resembles Figure 7b, but two important improvements are seen. First, the lower boundary and the resistivity of the thin top layer are smoothed out, resulting in a more homogeneous layer. Second, the artifacts occurring at the boundary between the second and third layers at profile coordinates 600 and 3400 in Figure 7b are removed. As indicated by the uppermost analysis section, the model-parameter determinations improve overall because of the prior information (i.e., the lateral smoothing) imposed in the correlation process. Thus, most of the model parameters are well defined, with the exception of the top-layer thickness. The bottom section shows the model-parameter analysis of the inverted models with prior information from the lateral correlation omitted. In this case, the uncertainties markedly increase, and the analysis section is comparable to Figure 7b.

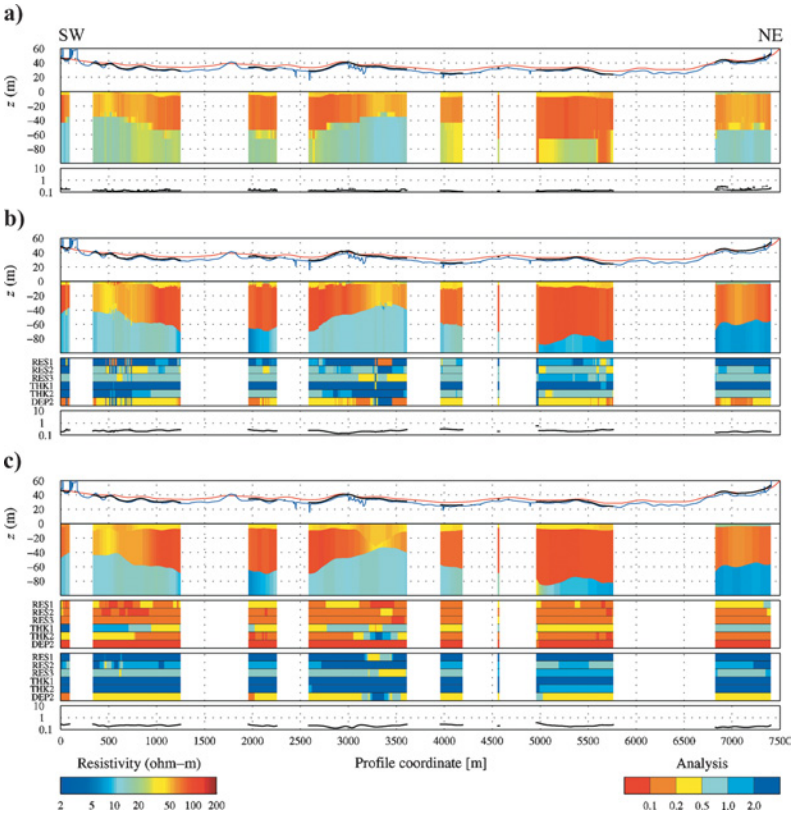

Figure 7. Resistivity sections along line 10 010, illustrating the different steps in the inversion scheme. (a) Multilayer inversion (step 1). (b) Few-layer inversion with extracted starting models (step 2) and model-parameter analysis of the inverted models. (c) Few-layer inversion with correlated starting models (step 3) and the model parameter analysis of the inverted models with and without prior information. The measured radar (red) and laser (blue) bird altitude is presented together with the inverted bird altitude (black) above each model section, and the total residual is presented below. Resistivities are indicated by the left color bar at the bottom, and the relative parameter uncertainties are indicated by the right color bar at the bottom.

DISCUSSION AND CONCLUSIONS

The HEM method is undoubtedly an efficient tool for geologic mapping. The question is whether it is also appropriate for hydrogeologic investigations where quantitative models and model-reliability specifications are required.

We have presented a theoretical study of the resolution capabilities of the DIGHEM^{VRES} system. The main results are summarized as follows:

- The effect of altimeter errors on the inversion results is serious, and even a small, 1-m error results in clearly disturbed output models. However, the problem can be avoided using an air-layer technique, with bird altitude entering the inversion as a highly resistive, at-surface layer thickness.
- The model-parameter determinations are only slightly reduced with the air-layer technique because the resistivity of the extra air layer is completely fixed and the thickness is very stable to resolve.
- The applicability for estimation of aquifer vulnerability is restricted because both the thickness and the resistivity of protective capping clay layers are poorly determined.
- In the best case, lower aquifer boundaries can be resolved to a depth of more than 100 m.

We have presented a new inversion scheme for multifrequency HEM data based on full nonlinear 1D inversion. The inversion scheme provides the best possible earth models supported by data-misfit parameters and quantitative model-parameter analysis of resolution. Tests on large-volume field data sets demonstrate that the inversion scheme is robust and reliable. The backbone of the inversion scheme is a multilayer inversion providing a good approximation of the true subsurface resistivity structures and reliable starting models for subsequent few-layer inversions. As part of the inversion scheme, a new method for correlation between separate 1D earth models along a profile has been introduced. The correlation procedure provides a fast technique for producing layered-model sections with only slow lateral variations. This characteristic is expected

in a sedimentary environment with slow, lateral variations in geology.

Finally, we have demonstrated that the EM coupling to a man-made conductor can have a serious impact on the measured data. Because of the deterministic character of cultural coupling, the coupling effect cannot be suppressed sufficiently by data filtering; thus, the data affected by cultural coupling must be removed before inversion to ensure valid output models. Optimally, the affected data should have been removed in the processing stage prior to filtering. Otherwise, an unnecessarily large part of the data must be removed because filtering blurs the cultural coupling laterally. The identification, registration, and removal of cultural couplings is time-consuming work, and an automatic procedure is desirable.

ACKNOWLEDGMENTS

The authors thank Ingelise Møller, Thorkild M. Rasmussen, and Kurt I. Sørensen, who participated in the work regarding the resolution capabilities of the HEM system. We acknowledge also the counties of Ringkjøbing and Storstrøm, whose generous cooperation made this study possible, and thank Fugro Airborne, owners of the DIGHEM^{VRES} system, for providing relevant system details. Finally, we are grateful to the editors and the three reviewers for their useful comments and suggestions.

APPENDIX A

EXTRACTION OF FEW-LAYER MODELS

In step two of the inversion scheme, the inverted multilayer models from step one are transformed into few-layer models. In this process, the (constant) number of layers L in the final few-layer models is decided. For each multilayer model, all possible L-layered submodels are then generated on the assumption that the layer boundaries must coincide with layer boundaries of the multilayer model. For each of the resulting submodels, the resistivity of the ith layer, consisting of layer k to l in the multilayer model, is derived as

$$\rho_i^{flm} = \exp\left(\frac{\sum_{j=k}^{l} \ln(\rho_j^{mlm}) d_j^{mlm}}{\sum_{j=k}^{l} d_j^{mlm}}\right), \tag{A-1}$$

where ρ_j^{mlm} and d_j^{mlm} are the resistivity and thickness, respectively, of the jth layer in the multilayer model. Next, each submodel is designated a number ε given by

$$\varepsilon = \sum_{j=1}^{M} (\ln \rho_j^{mlm} - \ln \rho_j^{flm})^2, \tag{A-2}$$

where M is the number of layers in the multilayer model and ρ_j^{flm} is the resistivity of the submodel in the depth interval corresponding to the jth layer of the multilayer model. The submodel that minimizes ε is finally selected as the best few-layer model.

APPENDIX B

LATERAL CORRELATION PROCEDURE

Techniques for lateral correlation of 1D earth models are presented in the literature by, e.g., Gyulai and Ormos (1999) and Auken et al. (2002). In this appendix we describe briefly the new correlation procedure referred to in the inversion scheme.

Having obtained a model section consisting of individually inverted few-layer models, all with the same number of layers, we perform the correlation on one model parameter at a time, e.g., the resistivity of the second layer. Correlation can be done on layer resistivities, layer thicknesses, or depths to layer boundaries. The values of the selected parameter for all models are collected in the parameter vector $\mathbf{p}$. The correlation is formulated as a constrained inversion problem, where $\mathbf{p}$ plays the role of the data vector and the model vector that we wish to find, $\mathbf{p}_{cor}$, is a smoother version of $\mathbf{p}$. The forward mapping between $\mathbf{p}$ and $\mathbf{p}_{cor}$ is given by

$$\mathbf{p} = \mathbf{p}_{cor} + \mathbf{e}, \tag{B-1}$$

where $\mathbf{e}$ is the observational error. The smoothing is realized by inverting relationship B-1 and incorporating a model covariance matrix $\mathbf{C}_m$ containing the elements

$$\mathbf{C}_m(i, j) = C_0 \exp(-r_{i,j}), \tag{B-2}$$

where $r_{i,j}$ is a normalized distance between the ith and the jth model positions and where C_0 is the correlation weight for the model parameter in question. The normalized distance $r_{i,j}$ is defined by

$$r_{i,j} = \sqrt{\left(\frac{x_i - x_j}{L_x}\right)^2 + \left(\frac{y_i - y_j}{L_y}\right)^2}, \tag{B-3}$$

with L_x and L_y the correlation lengths in the UTMX and UTMY directions, respectively. With no prior constraints on $\mathbf{p}_{cor}$, the inversion of equation B-1 then gives

$$\mathbf{p}_{cor} = \left(\mathbf{C}_p^{-1} + \mathbf{C}_m^{-1}\right)^{-1} \mathbf{C}_p^{-1} \mathbf{p}, \tag{B-4}$$

where $\mathbf{C}_p$ is a diagonal error covariance matrix of the uncorrelated parameters. Its elements are the variances of the parameters of the uncorrelated models.

The standard deviations of the correlated model parameters are finally found as the square root of the diagonal elements of the posterior covariance matrix $\mathbf{C}'_{est}$, given as

$$\mathbf{C}'_{est} = \left(\mathbf{C}_p^{-1} + \mathbf{C}_m^{-1}\right)^{-1}. \tag{B-5}$$

As mentioned, the inversion problem is solved for each resistivity and depth parameter separately. Generally, smoothing on depths is preferable to smoothing on thicknesses since continuity of depths is more relevant when considering a layered sedimentary environment (Auken and Christiansen, 2004). In the case of intersecting layer boundaries, a minimum layer thickness of 0.1 m is invoked. For large data sets, the inversion problem may become quite large and the solution thereby time consuming. This is, however, easily remedied by dividing the data set into smaller, overlapping segments of appropriate lengths.

As a consequence of the smoothing involved in the correlation process, the correlated models generally do not fit the data as well as the uncorrelated models. To remedy this without giving up the smoothness of the correlated models, a subsequent constrained inversion of the HEM data is performed with the correlated values $\mathbf{p}_{cor}$ as prior model parameters (the $\mathbf{m}_{prior}$ vector of equation 2) and a covariance matrix of the

prior values (the $\mathbf{C}_{prior}$ of equation 2) defined by the variances of $\mathbf{p}_{cor}$.

This method of lateral correlation of inverted models does not depend on data lying on a straight line or being equidistant because the model covariance matrix is based on the lateral distance between the models. It is also possible to correlate models obtained by inversion of different data types and to incorporate information form other sources, e.g., drill-hole information.

REFERENCES

Auken, E., and A. V. Christiansen, 2004, Layered and laterally constrained 2D inversion of resistivity data: Geophysics, **69**, 752–761.

Auken, E., N. Foged, and K. I. Sørensen, 2002, Model recognition by 1-D laterally constrained inversion of resistivity data: 8th Meeting, Environmental and Enginering Geophysics (EEGS-ES), Proceedings, 241–244.

Beamish, D., 2002a, An assessment of inversion methods for AEM data applied to environmental studies: Journal of Applied Geophysics, **51**, 75–96.

———, 2002b, The canopy effect in airborne EM: Geophysics, **67**, 1720–1728.

Beard, L. P., 2000, Comparison of methods for estimating earth resistivity from airborne electromagnetic measurements: Journal of Applied Geophysics, **45**, 239–259.

Christensen, N. B., and E. Auken, 1992, Simultaneous electromagnetic layered model analysis: GeoSkrifter, **41**, 49–56.

Christensen, N. B., and K. I. Sørensen, 1998, Surface and borehole electric and electromagnetic methods for hydrogeophysical investigations: European Journal of Environmental and Engineering Geophysics, **3**, 75–90.

———, 2001, Pulled array continuous electrical sounding with an additional inductive source: An experimental design study: Geophysical Prospecting, **49**, 241–254.

Christiansen, A. V., and N. B. Christensen, 2003, A quantitative appraisal of airborne and ground-based transient electromagnetic (TEM) measurements in Denmark: Geophysics, **68**, 523–534.

Danielsen, J. E., E. Auken, F. Jørgensen, V. Søndergaard, and K. I. Sørensen, 2003, The application of the transient electromagnetic method in hydrogeophysical surveys: Journal of Applied Geophysics, **53**, 181–198.

Farquharson, C. G., and D. W. Oldenburg, 1998, Non-linear inversion using general measures of data misfit and model structure: Geophysical Journal International, **134**, 213–227.

Fitterman, D. V., 1998, Sources of calibration errors in helicopter EM data: International Conference on Airborne Electromagnetics, Australian Society of Exploration Geophysicists, Proceedings 1.8.1–1.8.10.

Fraser, D. C., 1978, Resistivity mapping with an airborne multicoil electromagnetic system: Geophysics, **43**, 144–172.

———, 1987, Electromagnetic anomaly recognition within geologic and cultural noise, *in* T. G. Hildenbrand, G. L. Raines, and D. V. Fitterman, eds., National airborne geophysics programme: Developments and applications of modern electromagnetic surveys: U. S. Geologic Survey Bulletin, 1925, 53–64.

Gyulai, Á., and T. Ormos, 1999, A new procedure for the interpretation of VES data: 1.5-D simultaneous inversion method: Journal of Applied Geophysics, **41**, 1–17.

Hodges, G., 2003, Practical inversions for helicopter electromagnetic data: 15th Annual Symposium on the Application of Geophysics to Environmental and Engineering Problems (SAGEEP), Proceedings, 45–58.

Huang, H., and D. C. Fraser, 1996, The differential parameter method for multifrequency airborne resistivity mapping: Geophysics, **61**, 100–109.

Inman, J. R., 1975, Resistivity inversion with ridge regression: Geophysics, **40**, 798–817.

Jakobsen, T., E. Andersen, A. Nøddelund, A. Sonnenborg, A. Andesen, and T. Bjerre, 1997, Grundvandet i Storstrøms Amt (The groundwater in Storstrøms Amt): Storstrøms Amt Technical Report.

Menke, W., 1989, Geophysical data analysis: Discrete inversion theory: Academic Press Inc.

Poulsen, L. H., and N. B. Christensen, 1999, Hydrogeophysical mapping with the transient electromagnetic sounding method: European Journal of Environmental and Engineering Geophysics, **3**, 201–220.

Sengpiel, K.-P., 1988, Approximate inversion of airborne EM data from a multilayered ground: Geophysical Prospecting, **36**, 446–459.

Sengpiel, K.-P., and B. Siemon, 1998, Examples of 1-D inversion of multifrequency HEM data from 3-D resistivity distributions: Exploration Geophysics, **29**, 133–141.

———, 2000, Advanced inversion methods for airborne electromagnetic exploration: Geophysics, **65**, 1983–1992.

Siemon, B., 2001, Improved and new resistivity-depth profiles for helicopter electromagnetic data: Journal of Applied Geophysics, **46**, 65–76.

Siemon, B., C. Stuntebeck, K.-P. Sengpiel, B. Röttger, H.-J. Rehli, and D. G. Eberle, 2002, Investigation of hazardous waste sites and their environment using the BGR helicopter-borne geophysical system: Journal of Environmental and Engineering Geophysics, **7**, 169–181.

Sørensen, K. I., 1996, Pulled array continuous electrical profiling: First Break, **14**, 85–90.

Sørensen, K. I., and E. Auken, 2004, Sky TEM — A new high-resolution helicopter transient electomagnetic system: Exploration Geophysics, **35**, 191–199.